Purification of olive mill wastewater through noble metals nanoparticles synthesis: waste safe disposal and nanomaterials impact on healthy hepatic cell mitochondria

Valeria De Matteis[1]*, Loris Rizzello[2,3], Chiara Ingrosso[4], Rosaria Rinaldi[1]

1. Department of Mathematics and Physics "Ennio De Giorgi", University of Salento, Via Arnesano, 73100 Lecce, Italy
2. Institute for Bioengineering of Catalonia (IBEC), The Barcelona Institute of Science and Technology, Baldiri Reixac 10-12, 08028 Barcelona, Spain
3. Department of Pharmaceutical Sciences, University of Milan, via Mangiagalli 25, 20133 Milano, Italy
4. CNR-IPCF S.S. Bari, c/o Department of Chemistry, Università degli Studi di Bari, via Orabona 4-70126 Bari, Italy

*valeria.dematteis@unisalento.it

Phone/fax: +39 0832298108

Abstract

The exponential increase of waste derived from different human activities point out the importance of their reuse in order to create materials with specific properties, that can be used for different applications. In this work, it was showed how the typical Mediterranean organic liquid waste, namely Olive Mill Wastewater (OMWW), obtained during olive oil production, can be turned into an efficient reactive agent for the production of noble metals gold (Au) and silver nanoparticles (Ag NPs) with very well-defined physico-chemical properties. More than that, it was demonstrated that this synthetic procedure also lead to a drastic decrease of the organic pollution load of the OMWW, making it safer for environmental disposal and plants irrigation. Then, using healthy hepatic cell lines mitochondria, the biological effects induced by these green metal NPs surrounded by a polyphenols shell, with the same NPs synthetized through a standard chemical colloidal reduction process were compared, finding out that the green NPs are much safer.

Keywords: green synthesis; physico-chemical properties; mitochondria assessment; GTPase dynamin-related protein 1 expression; antioxidants perturbation; reusability of waste.

1. Introduction

Part of the Mediterranean area economy relays on the production of olive oil. Its extraction generates a solid waste, the Olive Mill Solid Waste (OMSW), along with a liquid part combined with wash-waters, named OMWW (Souilem et al. 2017). It is estimated that *c.a.* 30 million tons of OMWW are produced every year during the olive production period (from November to late February) in this geographical area (Dutournié et al. 2019). OMWW is slightly acid, and characterized by a high organic pollution loads, polyphenols and suspended solids (Aggoun et al. 2016; Torrecilla 2010). The organic pollution loads are mostly represented by chemical oxygen demand (COD), which is a measurement of the oxygen required to oxidize soluble and particulate organic matter. In OMWW, the COD values ranging between 45 and 170 g/L (Chatzisymeon et al. 2013; Chatzisymeon et al. 2009). These components are extremely toxic to the environment

and to the bacteria colonizing it (Chatzisymeon et al. 2009; Chatzisymeon et al. 2013). For instance, despite polyphenols have beneficial effects to human health due to their strong antioxidant properties, they are rather phytotoxic (Jillian 2017). It has been established that the impact of OMWW on the environment can reach the same levels as the whole pollution developed by a population of 22 million people in one year (Isidori 2005). Many chemical and physical methods have been thus employed to separate the organic phase from the OMWW in order to obtain a product that could be safely disposed in the environment or reusable for irrigation (Mantzavinos and Kalogerakis 2005; Mert et al. 2010; De Almeida et al. 2018). For example, the organic solvent-based extraction of polyphenols requires thermal concentration, ultrafiltration or lyophilisation steps (Torrecilla 2010). Other methods include supercritical fluid extraction (De Leonardis et al. 2014), evaporation and distillation (Rozzi 1996; Tsagaraki et al. 2007), neutralization/precipitation (Sarika et al. 2005) and electrocoagulation (Adhoum et al. 2004). In addition, also biological methods are used to remove polyphenols, like the use of bacteria (McNamara et al. 2008; Ramos-Cormenzana et al. 1996) or even nanoscaled materials such as Fe_2O_3 NPs (Nassar et al. 2014) and TiO_2 NPs (El Hajjouji et al. 2008; Nogueira et al. 2016) that were tested for their ability to reduce the COD values and the polyphenols from OMWW. Such latter approach, despite having intrinsic innovative aspects, has the limit to first optimise the chemical or physical synthesis and the characterization of NPs. However, although many methodologies have been employed to decrease the organic phase-related toxicity of OMWW (including NPs), further investigations are still needed to find the best approach for mitigating the OMWW environmental impact and to reduce the time consuming and expensive equipment (Rahmanian at al. 2014). In fact, not all mills can be equipped with expansive purification system, which are also require large facilities to host them. In a recent study, the polyphenols extracted from OMWW have been used as reducing agents to obtain magnesium oxide NPs (MgO NPs) (Hamimed 2020). It is well known that polyphenols (Singh et al. 2018) represent the most suitable reagents for the green production of NPs due to the high natural availaibility (especially in plant extracts). Also, they can act both as reducing and capping agents for the reduction of metal salts to obtain metallic NPs (1-100 nm) (Dauthal and Mukhopadhyay 2016; De Matteis et al. 2019; Bao et al. 2019). Here, a simple, direct and sustainable approach for the synthesis of metal NPs (Ag and Au) from an unprocessed/not-purified OMWW collected from a mill located in Southern Italy (Apulia) has been reported. The same NPs have been proved to significantly reduce, at the same time, the pollution load of OMWW. Highly stable colloidal Au and Ag NPs, with a size of ca. 20 nm and a surface coating of polyphenol molecules, have been produced. We demonstrated that the separated synthesis solution supernatant, namely the OMWW residue, shown significantly lower levels of polyphenols and COD. This confirmed the effectiveness of the synthetic procedure in sustainability, with the possibility to combine a green synthetic procedure with a reduction of waste toxicity in one shot, make it also suitable for irrigation. After the NPs green synthesis, the impact of the polyphenol-coated metal NPs on HL7702 human liver cell lines was assessed. The results were compared with these obtained using NPs, having the same chemical composition but synthesized through a standard colloidal chemical route, in order to assess any difference. The effects of the metal NPs on the mitochondrial membrane properties were investigated, in terms of potential, morphology, phospholipids and fatty acids content difference. The mitochondrial fusion process, that regulate cell growth, was studied following the expression of the GTPase dynamin-related protein 1 (Drp-1), which is recruited at the mitochondrial level to regulate fission step (Smirnova 1998). In addition, the levels of Reactive Oxygen Species (ROS) and Malondialdehyde (MDA) were estimated. Finally the cell cycle progression after exposure to the NPs through cytofluorimetric analyses were evaluated. The results shown that the Au and Ag NPs synthesized from OMWW had a very low impact on cells. To the best of our knowledge, it is the first time that OMWW is used to synthesize noble metal NPs, monodispersed in size and with quasi-regular morphology, without the implementation of time consuming and expensive steps to isolate

76　polyphenols from the organic pollution load. This approach opens new insights in the development of safe tools to apply
77　in nanomedicine.
78
79　**2. Materials and Methods**

80　**2.1 Reagents**

81　Tetrachloroauric(III) Acid ($HAuCl_4$), Silver Nitrate ($AgNO_3$), Sodium Citrate ($Na_3C_6H_5O_7$), Tannic Acid ($C_{76}H_{52}O_{46}$),
82　Folin & Ciocalteu's phenol reagent, Sodium Bicarbonate ($NaHCO_3$), Gallic Acid ($C_7H_6O_5$), Nitric Acid (HNO_3),
83　Hydrochloric acid (HCl), Anhydrous Acetone, DMEM (Dulbecco's Modified Eagle's Medium - high glucose), Fetal
84　Bovine Serum (FBS), Penicillin-Streptomycin, Dimethyl sulfoxide (DMSO), WST-8 ASSAY, Phosphate buffer saline
85　(PBS), Bovine Serum Albumin (BSA), hexane ($CH_3(CH_2)_4CH_3$), isopropanol ($(CH_3)_2CHOH$), chloroform ($CHCl_3$),
86　methanol (CH_3OH), Hydrogen Peroxide (H_2O_2), PhastGel® Homogeneous Pre-cast Gels 12.5 % polyacrylamide, 2′,7′-
87　Dichlorofluorescein diacetate (DCF-DA), 1X Tris-Buffered Saline, 0.1 % Tween® 20 Detergent (TBST) were purchased
88　from Merck KGaA, Darmstadt, Germany. HL7702 cells were purchased from ATCC (Manassas, VA, USA). Transfer
89　Buffer was purchased from Biorad. Lipid peroxidation assay kit (MDA) was purchased from ABCAM. MitoTracker™
90　Orange CMTMRos, JC1 dye and Mithocondria Isolation Kit were purchased from ThermoFisher Scientific, Waltham,
91　Massachusetts, USA. HPLC column was purchased from Phenomenex, BD Cycletest™ Plus DNA Kit was purchased
92　from BD Biosciences USA, primary rabbit antibody, Donkey anti-rabbit HRP 1:10000 and sheep anti-mouse HRP
93　1:10000 β-Actin were purchased from Novus Biological, Littleton, CO, 300 mesh amorphous carbon-coated Cu grids
94　were purchased from Ted Pella inc, USA.

95　**2.2 Green synthesis of the Au NPs and Ag NPs from OMWW**

96　The OMWW was collected in November from mill located in the Apulia region (south of Italy), and kept at −15 °C in
97　polyethylene bottles until use. The waste was kept at 4 °C in a dark sterile bottle to prevent biomolecules degradation.
98　The raw OMWW was purified by three cycles of centrifugation of 1 h at 6000 rpm to remove the solid part, and it was
99　filtered using Whatman filter paper n.1 (thickness 180 μm, pore size 11 μm). For the synthesis of the Au NPs, 5
100　mL of purified OMWW was added in a solution containing $HAuCl_4$ dissolved in MilliQ water (1 mM) in order to have a
101　1:4 ratio between OMWW and $HAuCl_4$ water solution. The mixture was left to stir (300 rpm) for 1 h at room temperature.
102　The same procedure was followed for the synthesis of the Ag NPs, in which $AgNO_3$ was used as precursor, after its
103　dissolving in MilliQ water (1 mM). During the synthesis of the Au NPs, the colour of the reaction solution turned from
104　light brown to wine red, and to dark brown, for the synthesis of the Ag NPs. After the two synthesis, the reaction solutions
105　were centrifuged for 1 h at 4000 rpm to separate the OMWW supernatant of the synthesis reaction solution from the pellet
106　containing the metal NPs. The OMWW supernatant was further analysed to determine COD levels, polyphenol content,
107　pH and electrical conductivity, whereas the pellet was purified with MilliQ water by three cycles of centrifugation, and
108　finally concentrated by an Amicon Ultra centrifugal 3k filter supplied by Merk, to assess the effect of the green metal
109　NPs on mitochondria of HL7002 cell lines.

110　**2.3 Synthesis of citrate-capped Au NPs and Ag NPs by conventional chemical routes**

111　The colloidal syntheses of the Au NPs and Ag NPs were performed according to the procedure described in (Maiorano et
112　al. 2013) and (De Matteis et al. 2015) which relay on the metal salt reduction in aqueous solution by using $Na_3C_6H_5O_7$.
113　For the Au NPs synthesis, a reaction flask, filled with 150 mL of 0.25 mM of $HAuCl_4$ aqueous solution, was heated up to

114   the boiling point under reflux while stirring, and then, 1.15 mL of 0.1 M $Na_3C_6H_5O_7$ was rapidly injected. The solution in

115   the flask was kept at the boiling point until the colour solution became red wine. For the synthesis of the Ag NPs, 1.5 mL

116   of $Na_3C_6H_5O_7$ aqueous solution (1.36 mM) containing 2.9 μM $C_{76}H_{52}O_{46}$ was heated up to 60 °C. After the addition of

117    $AgNO_3$ (0.592 mM) the solution was heated up to the boiling point until the colour turned to dark brown. The reaction

118   solutions were then cooled down to room temperature and stored in the dark at 4 °C. After this step, the achieved NPs

119   were centrifuged at 7500 rpm for 45 min and washed three times with MilliQ-water.

2.4 Inductively Coupled Plasma Atomic Emission Spectroscopy (ICP-AES)

121   The concentrations of the Au NPs and Ag NPs, synthetized through the OMWW and the colloidal routes, were calculated

122   by elemental analyses using ICP-AES and Varian Vista AX spectrometer (Varian Inc., Palo Alto, CA, USA). 250 μL of

123   the Ag NPs and Au NPs solutions were digested overnight, by adding 2 mL of HNO_3 and 2 mL of *aqua regia,* respectively,

124   followed by dilution with MilliQ water (1:5).

2.5 Morphology and spectroscopy investigation of the Au NPs the Ag NPs

126   TEM analyses were performed by using a Jeol Jem-1011 microscope operating at 100 kV, equipped by a high-contrast

127   objective lens and with a tungsten filament as electron source with an ultimate point resolution of 0.34 nm. Images were

128   acquired by a Quemesa Olympus CCD 11 Mp Camera. The samples useful for TEM observations were prepared by

129   depositing a drop (about 10 ul) of aqueous solution containing the metallic NPs on the carbon-coated grids. Once the

130   water evaporated, the grids were used for analysis. Size statistical analysis of the NPs average size and size distribution

131   was performed by using the fitting analysis available on OriginPro software. The DLS and ζ-potential acquisitions were

132   recorded by a Zetasizer Nano-ZS having a HeNe laser (4.0 mW) working at 633 nm detector (ZEN3600, Malvern

133   Instruments Ltd., UK) in aqueous solutions (25 °C,pH 7). NPs size statistical distribution of the NPs was measured on

134   300 Au NPs and Ag NPs fitted by a normal Gaussian function. UV-Vis-NIR absorption spectra of metal NPs solutions

135   were performed by Cary 5000 (Varian) UV/Vis/NIR spectrophotometer at room temperature. Varian 670-IR spectrometer

136   equipped by a DTGS (deuterated tryglycine sulfate) was used to acquire mid-infrared spectra. The spectral resolution of

137   detector was 4 cm^{-1}. For attenuated total reflection (ATR) measurements, a one-bounce 2 mm diameter diamond micro

138   prism was used as internal reflection element (IRE). The solutions were deposited directly by casting onto the upper face

139   of the diamond crystal and analysed after solvent evaporation.

2.6 COD measurement

141   The COD values of the pristine OMWW, the OMWW diluted in MilliQ water (1:4) and of the OMWW supernatant of

142   the Au NPs and Ag NPs synthesis solution, were measured according to the ISO 15705:2002 "Water quality—

143   Determination of the chemical oxygen demand index (ST-COD)" (Technical Committee : ISO/TC 147/SC 2 Physical,

144   2002) — Small-scale sealed-tube method). Such approach is based on the photometric determination, by the Fluorat-02

145   analyser, of the residual concentration of Cr(VI) ions after oxidation of the organic matter of the sample with an excess

146   of potassium dichromate in acid medium and in presence of sulphate silver.

2.7 Total Phenolic Compounds Content estimation

148   The Folin-Ciocalteu phenol reagent was used to measure the total phenolic content in pristine OMWW, the OMWW

149   diluted in MilliQ water (1:4) and of OMWW supernatant of the Au NPs and Ag NPs synthesis solution, following the

150   method previously described by Singleton and Rossi with some modifications. (Singleton and Rossi 1965) Briefly, 1.8 mL

4

151 of the Folin-Ciocalteu reagent and sodium bicarbonate (7.5 %) were successively added by 40 µl of OMWW at room

152 temperature. The mixture was kept in the dark for 1 h, and then, absorption spectra were recorded at 765 nm by using a

153 Jasco V-630 spectrophotometer. Gallic acid was used as standard phenolic compound for the calibration curve (r^2 =

154 0.9989). Total phenolic compound content is expressed as residual gallic acid equivalents (GAE) in gram per liter (gGAE

155 L^{-1}). Data were expressed as mean ± SD. Differences in total phenolic compounds between samples and controls were

156 considered statistically significant performing a student's t-test with a p values < 0.05 (<0.05 *, <0.01 **, and <0.005

157 ***).

2.8 Electrical conductivity (µS/cm) and pH

159 Electrical conductivity (µS/cm) and pH of OMWW, the OMWW diluted in MilliQ water (1:4) and supernatant of the

160 reaction solution of the green synthesized Au NPs and Ag NPs following the methods described in (CNR-IRSA, 2003).

161 Data were expressed as mean ± SD.

2.9 Chlorophyll a and Chlorophyll b determination in tomato plants (*Lycopersicon esculentum*)

163 The plants growth was made following the procedure described in (Daâssi et al 2016) with some modifications. Briefly,

164 the tomato seeds were sown on in alveolus plates filled with peat for 3 weeks. The seedlings were successively transferred

165 into pots (three plants per pot) including 500 g of peat and located to a greenhouse. After 10 days, the plants were first

166 fertilized and, after 3 days, they were irrigated weekly for three weeks with 10 mL of pristine OMWW, the OMWW

167 diluted in MilliQ water (1:4) and the OMWW supernatant derived from Ag NPs and Au NPs synthesis were used. We

168 used three blocks and three replicates. The treatment with water was the control. In addition, the pH of OMWW was

169 adjusted to 7.0 in order to eliminate alteration induced by acidity. The MacKinney approach (MacKinney et al 1941) was

170 used to record the amount of Chlorophyll a (Chl a) and Chlorophyll b (Chl a) in tomato plants. After 3 weeks of irrigation,

171 starting from the same plants height (*c.a.* 30 cm), 7 mg of fresh leaves were crushed into small portions and moved in 1.5

172 mL of anhydrous acetone following two-centrifugation steps of 14.0000 rpm for 15 minutes (4°C). The supernatant

173 recovered was analysed at 645 and 663 nm (Lichtenthaler et al 2001). Data were expressed as milligrams per gram of

174 fresh weight of tomato ± SD. Differences between samples and control were evaluated performing a student's t-test and

175 were considered statistically significant for p values < 0.05 (<0.05 *, <0.01 **, and <0.005 ***). **2.10 Cells culture**

176 HL7702 cells were grown in Dulbecco's modified eagle's medium (DMEM) added by 10 % FBS and 1 % antibiotic-

177 antimycotic solution at 37° C in a humidified incubator with 5 % CO_2. In order to evaluate the mitochondria membrane

178 composition, cells were harvested during the exponential phase of growth at 80 % of confluence, starting from 25 million

179 cells.

2.11 Cells viability assessment by WST-8 Assay

181 5×10^3 HL7702 cells/ well were seeded in 96 well microplates. After 24 h, cells were exposed for 24 h and 48 h to two

182 concentrations of polyphenol- and citrate-capped Au NPs and Ag NPs stock solutions, namely 10 µg mL^{-1} (c1) and 25 µg

183 mL^{-1} (c2). DMSO was used as positive control (data not shown). At the endpoints, cell viability was investigated by using

184 a standard WST-8 assay following the procedure previously described (De Matteis et al 2017). Differences in cell viability

185 between cells treated with NPs and the control were statistically significant performing a student's t-test with a p values

186 < 0.05 (<0.05 *).

2.12 Mitochondrial membrane potential analysis by JC1 dye

188 HL7702 cells were seeded in dark 96 well microplates and treated for 24 h and 48 h with c1 and c2 polyphenol- and
189 citrate-capped Au NPs and Ag NPs. Then JC-1, a cationic carbocyanine dye, was used to measure the mitochondrial
190 membrane potential. . After NPs exposure, the medium was removed and cells, firstly washed with PBS buffer solution,
191 were incubated with JC-1 (2.5 µg mL^{-1}) for 2 h. Once removed the dye, cells were washed with PBS in order to remove
192 the excess of dye. Then, the cells fluorescence was detected from each well using Bio-Rad Fluo Star Optima (BMG
193 LABTECH) microplate spectrophotometer. Results were normalized with respect to negative controls expressed as 100
194 %. As positive control, cells were incubated with 100 µM valinomycin. Data are reported as mean values ± SD. The
195 difference between cells treated with NPs and controls was considered statistically significant performing a student's t -
196 test with a p values < 0.05 (< 0.05 *)

2.13 Mitochondria isolation, proteins and lipids extraction of mitochondrial membranes.

198 The isolation of mitochondria from HL7702 cells was performed, before and after 24 h and 48 h of treatment with c1 and
199 c2 polyphenol- and citrate- capped Au NPs and Ag NPs, starting from 1×10^7 cells following the procedure described in
200 Mitochondria Isolation Kit. The procedure was based on Dounce homogenization. The further isolation was carried out
201 by differential centrifugations to separate the mitochondria. In particular the centrifugation at 3000 × g for 10 min at 4°C
202 permitted to obtain mitochondria in the pellet that were wash and successively centrifuged at 12000g for 5 min at 4 °C.
203 The step at 3000 x g allows the collection of highly purified mitochondria. The typical yield relays on ca. 150 µg protein
204 from 20 million starting cells. Highly purified proteins will be subsequently achieved from mitochondria after applying
205 lysis buffer containing a protease inhibitor. The protein amount of the mitochondrial fraction was determined by a
206 Bradford protein assay using BSA protein as standard (Bradford, 1976). Lipids were extracted and purified according to
207 Bligh and Dyer procedure (Bligh and Dyer 1959).

2.14 Separation of phospholipids by High Performance Liquid Chromatography (HPLC) and quantitative analysis by phosphorus dosage

211 Mitochondrial phospholipids from HL7702 cells were separated by HPLC, before and after 24 h and 48 h of treatment
212 with c1 and c2 polyphenol- and citrate-capped Au NPs and Ag NPs.
213 The column, 250 x 4.6 mm in size, with a stationary phase formed of an orthosilicic acid polymer was used. The elution
214 of the phospholipids was carried out in a gradient by the use of two phases, namely phase A relaying on a
215 $(CH_3(CH_2)_4CH_3):(CH_3)_2CHOH$ (6:8 % v/v) solution, and phase B relaying on a $(CH_3(CH_2)_4CH_3):(CH_3)_2CHOH:water$
216 (6:8:1.4 % v/v) solution. After 15 min the chromatographic peaks of the eluted phospholipids were detected by HPLC
217 detector absorption spectra, collected by LKB 2238 Uvicord SII uv monitor and equipped with a 206 nm interference
218 filter. The assignment of the phospholipids was performed by the absorption signal at 206 nm related to the –C=C- bonds
219 of the fatty acid chains (Holte LL et al. 1990). The phospholipids of the sample were identified by comparing the retention
220 times with those of the added standards.
221 The phospholipids quantitative analysis was carried out by the phospholipid phosphorus dosage by using the Nakamura
222 method (Nakamura 1952) and the Fiske reagent (Fiske 1925). The values of the phospholipidic phosphorus were obtained
223 spectrophotometrically, extrapolating the absorbance of the sample solutions from the calibration curve, divided by the
224 atomic weight of the phosphorus, and then multiplied by the average molecular weight of the phospholipids (870 Dalton).
225 The quantity of the phospholipids was reported as µg of phospholipid phosphorus/mg of mitochondrial proteins.

2.15 Mitochondrial fatty acids composition

The fatty acids composition of purified mitochondria from HL7702 cells was determined according to the procedure described in Ichihara et al. (2010). Lipids were extracted from the mitochondria with chloroform/methanol (2:1 % v/v) solution and then methylated with 0.5 M HCl in methanol (0.5 M). Fatty acid methyl esters were separated and quantified by gas chromatography.

2.16 Immunoblot analysis

The mitochondrial fission regulator Drp-1 levels in HL7702 cells were estimated by immunoblotting, before and after treatment with c2 polyphenols- and citrate-capped Au NPs and Ag NPs for 48 h. The protein lysates were separated by using 12.5 % sodium dodecyl sulfate polyacrylamide gel electrophoresis (SDS-PAGE 12.5 %) and soaked in Transfer/Towbin buffer for 15 min. After the separation, the proteins were transferred onto a nitrocellulose membrane, blocked with 5 % BSA in a TBS/Tween, and then incubated with primary antibodies at 4 °C overnight. The nylon membranes were incubated overnight with the primary antibodies. After incubation, the membrane was rinsed three times with Tris-buffered saline (TBS) and Polysorbate 20 (Tween 20, TBST) and incubated with the appropriate secondary antibody, namely donkey anti-rabbit HRP 1:10000 (Novus Biological, Littleton, CO) for the DPR-1 protein, and sheep anti-mouse HRP 1:10000 β-Actin (Novus Biological, Littleton, CO) for β-actin, followed by three additional rinses performed at intervals of 10 min. Relative band intensities were recorded by densitometry, normalizing the band intensities of the untreated samples to that of the β-actin signal.

2.17 Determination of ROS production by DCF-DA Assay

HL7702 cells were seeded in 96-well microplates and treated for 24 h and 48 h, by the polyphenol- and citrate-capped Au NPs and Ag NPs at the c1 and c2 concentrations. After cell–NPs interaction, the DCF-DA assay was performed following the procedure reported elsewhere (De Matteis et al. 2019). As a positive control, cells were exposed to 500 μM H_2O_2 that induced an increase of fluorescence of about 300 % due to the ROS formation. Data are reported as mean values ± SD estimated from three independent experiments. The difference between cells treated with NPs and controls was considered statistically significant performing a student's t-test with a p values < 0.05 (<0.05 *).

2.18 Lipids peroxidation by Malondialdehyde (MDA) quantification

HL7702 cell extracts were prepared according to the procedures described in De Matteis et al (2019). The assay was performed on microplates by applying the Lipid Peroxidation (MDA) Assay kit, in which the MDA of the sample reacts with thiobarbituric acid (TBA) to generate the MDA-TBA adduct and the concentration (nmol mg^{-1} protein) of the MDA-TBA adduct was determined from the absorbance spectra at 532 nm, by using a Bio-Rad microplate spectrophotometer. Data are reported as mean values ± SD estimated from three independent experiments. The difference between cells treated with NPs and controls was considered statistically significant performing a student's t-test with a p values < 0.05 (<0.05 *).

2.19 Mitochondrial morphology investigation by confocal microscopy and ImageJ software analysis

HL7702 cells were exposed for 48 h to c2 polyphenol- and citrate-capped Au NPs and Ag NPs. After incubation, the medium containing NPs was replaced with PBS. After this step, the cells were washed several and 300 nM mL^{-1} MitoTracker™ Orange CMTMRos was used to label mitochondria. After an incubation of 20 min in the incubator, Confocal acquisitions were collected by the Leica TCS SPE-II confocal microscope, using a 100X objective (water immersion, HCX PL APO, 1.10NA). Mitochondrial average circularity, mitochondria area/perimeter normalized to

264   circularity and mitochondria area/perimeter normalized to minor axis were measured on 20 cells by means of the ImageJ

265   1.47 analysis software. The difference between cells treated with NPs and controls was considered statistically significant

266   performing a student's t-test with a p values < 0.05 (< 0.05 * < 0.01 ** and < 0.005 ***).

267   **2.20 Cell cycle analysis**

268   Following trypsinization, HL7702 cells (before and after 48 h of treatment with c2 polyphenols- and citrate-capped Au

269   NPs and Ag NPs) were adjusted to a concentration of 1×10 cells/mL and treated using Cycle TEST^{TM} PLUS DNA Reagent

270   Kit according to the manufacturer's instructions. The cell cycle was analysed by flow cytometry using propidium iodide

271   (PI). FACSCalibur (Becton Dickinson, CA) was used for data acquisition and analysis to determine cells percentages in

272   the cell cycle phases sub G0/G1, G0/G1, S, and G2/M.

273

274   **3. Results and discussion**

275   OMWW is usually produced in tons during the period of olive oil production. The high percentage of polyphenols and

276   extremely polluting COD values characterizing it, makes the disposal very challenging. Here, we showed the possibility

277   of using OMWW for the green synthesis of metal NPs, a process that also induced a significant decrease of the pollution

278   load in the OMWW resulting from the synthesis. Au and Ag NPs were synthetized by adding 1 mM of metal salts ($AgNO_3$

279   and $HAuCl_4$) aqueous solutions to OMWW. The TEM images shown multifaceted anisotropic nanostructures, some

280   triangular/hexagonal objects and nearly-spherical NPs (**Figure 1 a,b**). The ImageJ software was used to record the mean

281   size distribution on TEM acquisitions, that were 21 ± 7 nm and 19 ± 8 nm for Au and Ag NPs, respectively. The statistical

282   analysis was performed on 100 of each NPs type, and the red line represented the Gaussian fitting (**Figure 1 c,d**). The

283   nano-objects were coated by a low contrast organic shell reasonably ascribed to the polyphenols, involved in the metal

284   salts reduction in solution (Alegria et al. 2018), and concomitantly acting as coordinating and stabilizing agents of the

285   forming NPs. DLS measurements confirmed the TEM data, observing an hydrodynamic radius of 20 ± 8 nm and 20 ± 7

286   nm for the Au (**Figure 1e**) and the Ag NPs (**Figure 1f**), respectively. Similar surface charge of -48 ± 3 mV (**Figure g**)

287   and -45 ± 4 mV mV (**Figure h**) were also quantified. Conversely, the DLS measurements of the citrate-capped Au and

288   Ag NPs, synthetized by the standard chemical route, had a hydrodynamic diameter of 20 ± 6 nm and 21 ± 3 nm,

289   respectively. In addition, their surface charge was -32 ± 3 mV and -25 ± 5 mV respectively (**Table 1**).
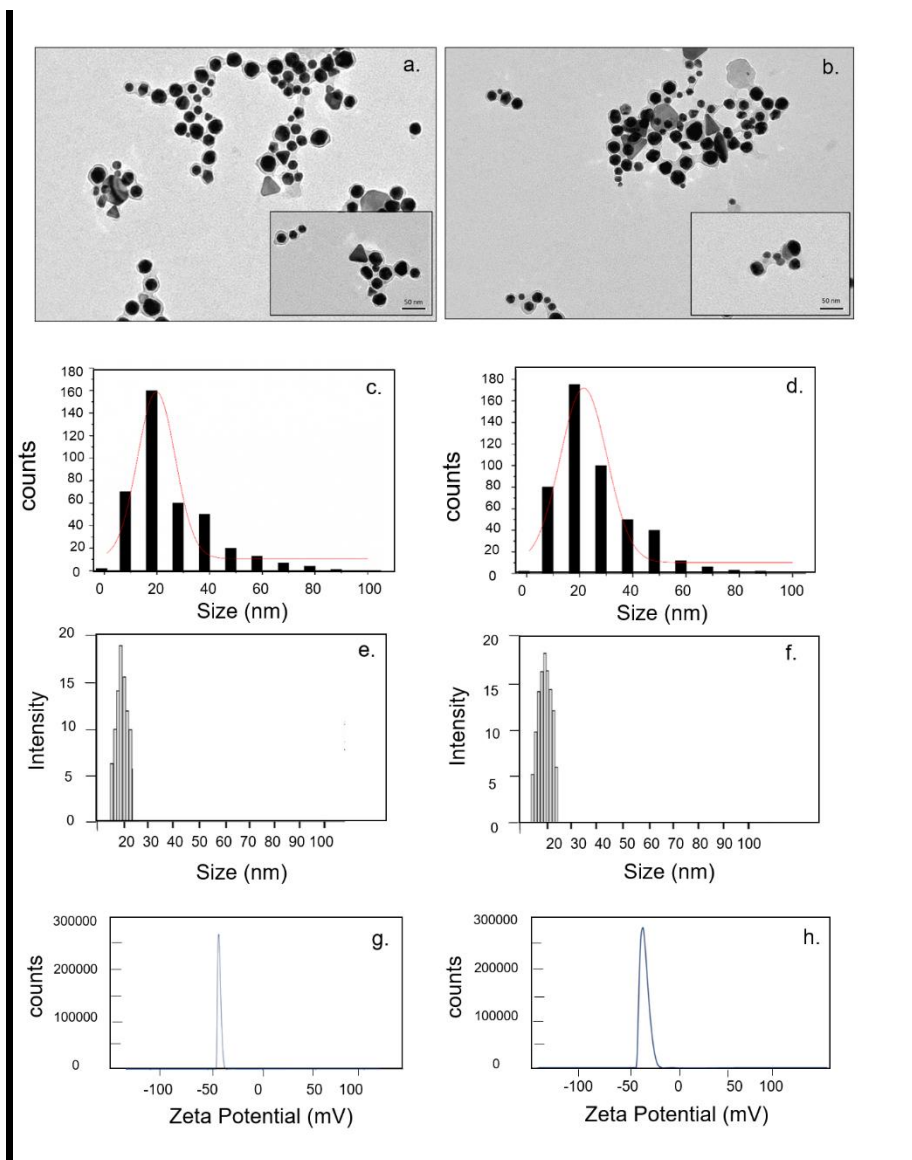
Figure 1. TEM images and size distribution obtained from ImageJ of polyphenol-coated Au NPs (**a,c**) and Ag NPs (**b,d**). DLS spectra (**e-f**) and ζ-potential (**g-h**) of Au NPs (**e,g**) and Ag NPs respectively (**f,h**).

Samples	Size (nm)	ζ-potential (mV)
Au NPs	20 ± 6	-32 ± 3
Ag NPs	21 ± 3	-25 ± 5

Table 1. NPs mean sizes recorded by DLS and ζ-potential values of citrate-coated Au NPs and Ag NPs.

The UV-Vis-NIR absorption spectra of the OMWW-derived Au and Ag NPs showed an intense absorption band in the UV region (**Figure 2a**) at ca. 230 nm, accounted for by the π-π* transition of the conjugated carbon bonds of aromatic phenolic compounds. In addition, a Localized Surface Plasmon Resonance (LSPR) absorption band peak was observed

9

at 431 and 545 nm for Ag and Au NPs, respectively (**Figure 2 a**). **Figure 2b** reported the FTIR-ATR spectra of the OMWW starting solution comparing it with the spectra of polyphenols-capped Au NPs and Ag NPs. The infrared spectrum of OMWW shown, in the high wavenumber region, a broad band between 3650 and 3000 cm^{-1} corresponding to the –OH stretching mode (v-OH), along with peaks at 2924 cm^{-1}, 2884 cm^{-1} and 2854 cm^{-1}, accounted for by the -CH$_2$ asymmetric stretching (vas-CH$_2$) and the -CH$_3$ and -CH$_2$ symmetric modes (vs-CH$_2$, vs-CH$_3$) of polyphenolic compounds. In the low wavenumber region, OMWW shown a broad band at 1708 cm^{-1}, which can be likely accounted for by –C=O stretching vibration (v-C=O) of carboxylic acid groups, as well as, a broad band at 1666 cm^{-1}, likely accounted for by –C=C- stretching modes (v-C=C-) of vinyl ether groups, and a band at 1587 cm^{-1}, reasonably due to –C=C- stretching vibrations of the aromatic ring of phenols, ethers and benzoic acids. Finally, in the finger print region, the –OH bending mode (δ-OH) at 1396 cm^{-1} and the –C-O stretching vibrations (v-C-O) of carboxylic acid groups at 1260 cm^{-1} can be observed, as well as –C-O-C- stretching vibrations of aromatic and vinyl ether moieties (v-C-O-C-) at 1068 cm^{-1} and –C-O stretching modes of aromatic alcohols (v-C-O) at 1031 cm^{-1}, can be detected. The infrared spectrum profile of the Au NPs and Ag NPs looked very similar and presented, in the high wavenumber region, the same broad bands detected in the spectrum of OMWW, likely accounted for by the –OH (v-OH) and alkyl (vs-CH$_2$, vs-CH$_3$) stretching modes of the polyphenolic compounds extracted from OMWW in the synthesis process. Conversely, in the low wavenumber region, the metal NPs shown the vibrations at 1742 cm^{-1} and 1642 cm^{-1}, mainly ascribed to the –C=O stretching vibration (v-C=O) of ester groups and the –C=C- stretching modes (v-C=C-) of aliphatic vinyl ethers. In the finger print region, the bands at 1455 cm^{-1} and 1417 cm^{-1}, likely ascribed to the –C=C- stretching band (v-C=C-) of aromatic benzyl alcohol groups and to the –CH bending (δ-CH) of aliphatic groups, respectively can be observed. Finally, the vibrations at 1233 cm^{-1}, 1209 cm^{-1}, 1163 cm^{-1}, 1108 cm^{-1}, 1038 cm^{-1} and 850 cm^{-1}, can be likely ascribed to the –C(=O)-O- stretching (v-C(=O)-O) of ester moieties, the -O-H bending (δ-OH) of benzyl alcohols groups, the -O-C-C- stretching (v-O-C-C-) of ester groups, the –C-O-C- asymmetric stretching (vas-C-O-C) of ether groups, the C-O stretching (v-C-O-) of benzyl alcohols, and the aromatic ring -C-H bending (δ-CH), respectively. These evidences suggested that the polyphenols derived from OMWW reasonably involved in the coordination of the metal NPs surface as observed in the TEM images of Figure 1 a and b, and hence, they were responsible for the long-term colloidal stability of the nano-objects in water.
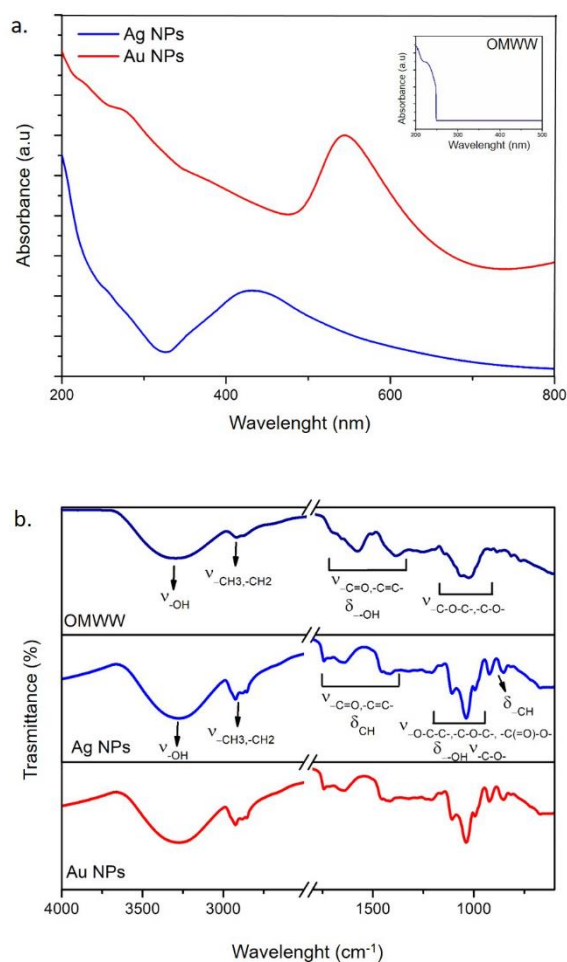
Figure 2. (a) UV-Vis-NIR and (b) FTIR-ATR spectra of OMWW and polyphenol-capped Ag NPs and Au NPs.

The OMWW chemical composition depends on the variety of olive, stage of maturity, storage time, climate (Niaounakis et al. 2006); the high levels of COD (up to 170 g/L) and polyphenols (up to 24 g/L) limit the waste disposability. Therefore, the COD levels and total polyphenol contents of pristine (as collected) OMWW, of OMWW diluted with milliQ water (1:4) (namely the same dilution used for the green synthesis of the metal NPs), and of the OMWW supernatant of the polyphenol-coated Ag NPs and Au NPs synthesis reaction, have been measured. The results showed that the pristine OMWW presented a high level of COD corresponding to 169 ± 13 gO_2 L^{-1}, which decreased down to 42 ± 15 gO_2 L^{-1} after the dilution with milliQ water (ratio 1:4). Remarkably, a significant decrease of the COD content to 3.2 ± 1.5 gO_2 L^{-1} and 3.8 ± 1.3 gO_2 L^{-1} was observed after the green synthesis of the Au and Ag NPs, respectively (**Figure 3 a**). The total polyphenols content of pristine OMWW was 25 ± 8 gGAE L^{-1} and became 13 ± 3 gGAE L^{-1} after the 1:4 dilution, significantly decreasing down to 2.0 ± 0.2 gGAE L^{-1} and 3.1 ± 0.4, after the synthesis of the Au NPs and Ag NPs (**Figure 3 b**).
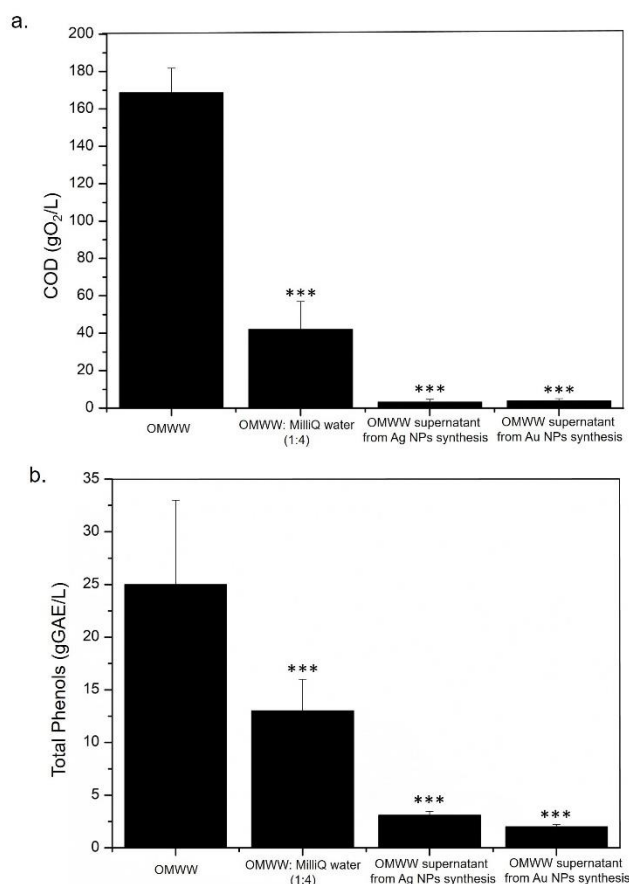
11

341

Figure 3. COD (**a**) and total polyphenols content of OMWW, OMWW: MilliQ water (1:4) and OMWW supernatant derived from the Ag and Au NPs green synthesis.

The electrical conductivity and the pH of OMWW were measured as well. For the OMWW sample, an electrical conductivity of 5980 ± 1200 μS cm^{-1} and a slightly acid pH of 5.02 were found. The conductivity was reduced down to 1154 ± 510 μS cm^{-1}, while an increase up to 5.23 in pH after the water 1:4 dilution was observed. The conductivity of the OMWW supernatant derived from green Ag and Au NPs synthesis reduced down to 1004 ± 458 μS cm^{-1} and to 390 ± 169 μS cm^{-1} (**Table 2**), respectively, with a slight change of pH as well to 4.85 and 4.98.

Samples	Electrical conductivity (μS cm^{-1})	pH
OMWW	5980 ± 1200	5.02
OMWW: MilliQ water (1:4)	1154 ± 510	5.23
OMWW supernatant from Ag NPs synthesis	390 ± 169	4.85
OMWW supernatant from Au NPs synthesis	1004 ± 458	4.98

350

Table 2. Electrical conductivity and pH values of OMWW, OMWW: MilliQ water (1:4) and OMWW supernatant derived from the Ag and Au NPs green synthesis.

12

The analysis of the OMWW supernatant isolated from the synthesis reaction of the metal NPs showed a significant reduction of COD and total polyphenols amount. Herein, the synthesis of the noble metal NPs was performed without any extraction of the polyphenols, as instead already demonstrated elsewhere for MgO NPs (Hamimed et al. 2020). More importantly, the *in situ* synthesized metal NPs were able to extract such polluting compounds from OMWW, allowing its possible safe disposal in the environment, or its use as irrigation source (Enaime et al. 2020). In fact, it has been previously demonstrated that the purified OMWW increased soil fertility (Flouri et al. 1988) resulting effective as fertilizer for olive trees, grapes and potatoes (Balis et al. 1995) stimulating plants growth enhancer, as well (Rusan et al. 2016). To assess the possible use of purified OMWW on plants as irrigation source, we evaluated the leaves pigmentation exerted by Chlorophyll a (Chl a) and Chlorophyll b (Chl b) on tomato plants (*Lycopersicon esculentum*) after their irrigation for three weeks with water. Pristine OMWW, the OMWW diluted in MilliQ water (1:4) and the OMWW supernatant derived NPs synthesis were tested. The results showed that the total amount of Chl a and Chl b significantly increased upon treatment with the supernatant OMWW derived from Ag NPs and Au NPs synthesis finding values of 173 ± 7 mg/g and 176 ± 6 mg/g respectively. Conversely, the plants irrigation using pristine OMWW and the relative dilution in water (1:4) showed very low values (41 ± 4 mg/g and 85 ± 9 mg/g) with respect to the use of water (120 ± 10 mg/g) (**Supplementary Material, Figure 1S**). As previously reported (Ouzounidou and Zervakis 2010), the reduction of Chlorophyll content in tomato leaves irrigated with pristine OMWW could be due to polyphenols interference in the Chlorophyll formation and its pollutant charge. The supernatant OMWW presented a negligible concentration of polyphenols. These results were in accordance with other works that reported that purified OMWW enriched poor soils and, at the same time, it increased the leaves pigmentation. (López-Piñeiro et al. 2007). We then moved on studying the effects of the polyphenol-capped Au NPs and Ag NPs on the mitochondria of HL7702 liver cells comparing them with the effects caused by the citrate-capped Au and Ag NPs (also having same size), synthesized through a standard reduction chemical route.

Firstly, the cells viability after 24 h and 48 h of exposure to polyphenol-capped Au NPs and Ag NPs at the two concentrations, c1 and c2 were assessed. Significant differences were observed in the cell viability after treatment with either the polyphenol- and the citrate-coated NPs. The polyphenol-capped NPs did not reduce the cell viability to values below 70 % (compared to control untreated cells) even after 48 h of exposure to the highest concentration tested. A value of 70 ± 12 % was found for highest concentration of Ag NPs after 48 h, whereas the cell viability upon treatment with Au NPs was 78 % ± 9 (**Figure 4A**). On the other hand, the citrate-capped Ag NPs showed the highest toxicity after 48 h of exposure to the c2 concentration, at which only the 43 % of cells remains vital. The citrate-capped Au NPs drastically reduced cell viability to 52 %. The effect of the polyphenol-coated metal NPs on the HL7702 liver cells was further studied by investigating mitochondria (*i*) membrane potential (MMP), (*ii*) phospholipid/fatty acids content and morphology (*iii*). The maintenance of MMP is critical for cell viability, as it is based on the pumping of hydrogen ions across the inner membrane during electron transport and oxidative phosphorylation, that is the driving force for the physiological ATP production (Acton et al. 2004). Any modification of the MMP values have been investigated by monitoring changes of the photoluminescence emission of the molecular label JC-1. This dye reagent crosses the mitochondrial membrane and possesses a green fluorescence emission peak at ~530 nm. Upon variation in the MMP, the dye is not able to accumulate in the organelle and it forms J-aggregates that exhibit a broad excitation spectrum and an emission maximum at ~590 nm. The exposure to citrate-coated Ag NPs (c2) for 48 h reduced the MMP value of 60 %, whereas the MMP did not undergo significant changes after exposed cells to the polyphenol-capped NPs, demonstrating high tolerance towards these NPs. In agreement with viability results, these effects were particularly evident after 48 h of exposure to the c2 citrate-coated Ag NPs (**Figure 4b**).
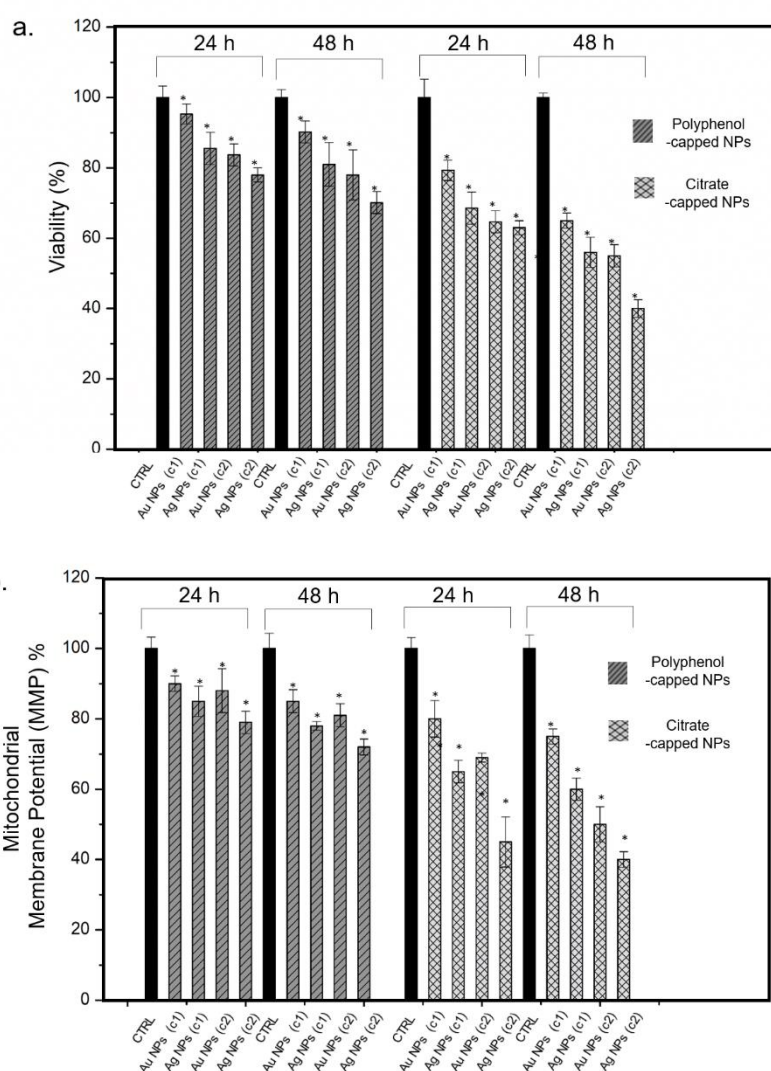
13

Figure 4. **a.** Viability (WST-8) assay of HL7702 cells after 24 h and 48 h of exposure to c1 and c2 polyphenol-capped and citrate-coated Au NPs and Ag NPs. Viability of NPs-treated cells normalized to non-treated control cells. **b.** Effect of 24 h and 48 h exposure to c1 and c2 polyphenol-capped and citrate–coated Au NPs and Ag NPs on MMP in HL7702 cells. Cells were incubated with 2.5 µg mL^{-1} JC1 and cell fluorescence was collected from each well. The % MMP of NPs-treated cells is expressed relative to non-treated control cells.

The alteration of the MMP can be due to integrity loss of the outer and inner side of the mitochondrial membrane. Here phospholipids like cardiolipin (CL), phosphatidylethanolamine (PE), phosphatidylinositol (PI), phosphatidylserine (PS) and phosphatidylcholine (PC) play a fundamental role in preserving the membrane structure. Among these phospholipids, PC is the most abundant in the outer membrane layer, whereas CL is the typical phospholipid of the inner mitochondrial membrane, responsible for the chain function of electron transport. A decrease in CL content destabilize the complex III and IV of the respiratory cellular chain, thus triggering the caspases activation and leading to apoptosis (Kagan et al. 2005; Yin et al. 2012). In addition, it has been demonstrated previously, that its alteration is implicated in several human diseases, such as atherosclerosis (Berliner and Leitinger 2009), cancer (Hammad et al. 2009), Barth syndrome (Barth et

14

al. 1983), and neurodegenerative disorders (Montine et al. 2005). Any possible changes in the phospholipids phosphorus content in mitochondrial membranes of HL7702 cells were then investigated, observing significant effects after 48 h of exposure to c2 NPs. After cell incubation with polyphenol- and citrate-capped Au NPs and Ag NPs, mitochondria were isolated by differential centrifugation steps and phospholipids were separated by HPLC. We observed a general trend of decrease in phospholipids content, as it can see in total chromatograms of mitochondrial phospholipids, especially after treatment with citrate-coated Au NPs and Ag NPs, and the highest reduction has been observed for CL, PE and PC (**Figure 5a**). CL values changed from 10 ± 1.3 µg mg^{-1} for the control to 9.1 ± 2.1 µg mg^{-1} and 8 ± 1.8 µg mg^{-1} after treatment with the polyphenol-capped Au NPs and Ag NPs, respectively. These values corroborated the results obtained for the MMP analyses, confirming that the polyphenol-capped NPs did not significantly affected the CL levels, as well as the other phospholipids. The PC levels slightly changed after incubation with the polyphenol-capped Ag NPs, passing from the control value of 59.6 ± 14 µg mg^{-1} to 54 ± 11 for Au NPs and 44.4 ± 12 µg mg^{-1} for Ag NPs. Conversely, the exposure to the citrate-coated NPs was found to trigger a significant alteration of phospholipids content. The CL decreased down to values of 2 ± 0.3 µg mg^{-1} after 48 h of exposure to c2 citrate-coated Ag NPs, and to 5.2 ± 2 µg mg^{-1} after exposure to Au NPs. Similarly, the levels of PC decreased to 3.5 ± 1.5 µg mg^{-1} after cells incubation with citrate-coated Ag NPs (**Figure 5b**).
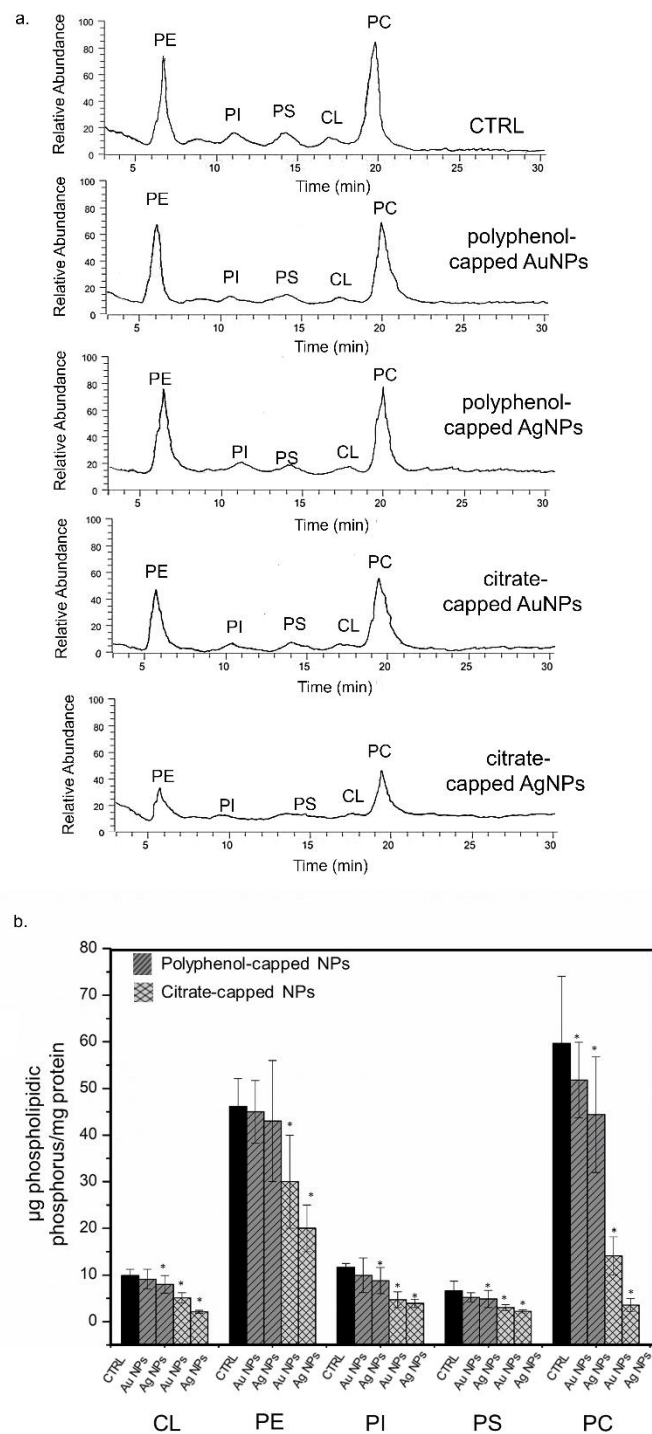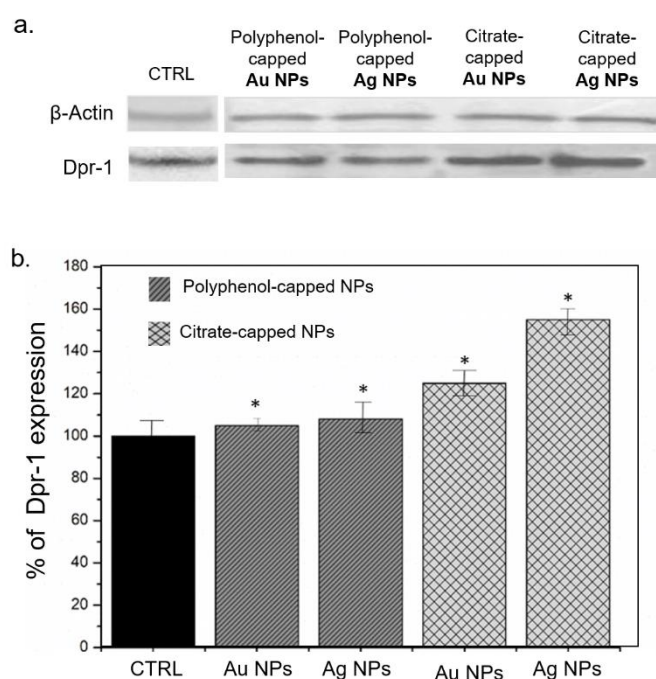
Figure 5. **a.** Total chromatograms of mitochondrial phospholipids separated by HPLC in mitochondrial membranes of HL7702 cells induced by 48 h of exposure to c2 polyphenol- and citrate-capped Au NPs and Ag NPs and **b.** the relative phospholipids quantitative analysis expressed as µg phospholipids phosphorus/mg protein, Results are calculated as mean of five experiments ± DS and they considered statistically significant performing a student's t-test with a p values < 0.05 (<0.05 *).

These data highlighted how the NPs produced by the colloidal route, and the Ag NPs in particular, were responsible for the most significant modifications. This result can be due to the peroxidation of acyl chains of phospholipids; for this reason, the amount of these acylic chains was carefully analysed, observing a general decrease in the content of both the saturated and unsaturated fatty acids, evident when cells were exposed to citrate-coated NPs derived. Conversely, the polyphenol-capped NPs induced negligible effects on the fatty acid content, probably due to the polyphenolic shell. It is reasonably that the phytocompounds act as antioxidant in several diseases involving the genes responsible of the fatty acid chains elongation. (Sha 2018). Remarkable changes in the levels of saturated (Myristic, Palmitic and Stereatic) and unsaturated (Palmitoleic, Oleic, Linoleic, Arachidonic, Eicosapentaenoic, Docosapentaenoic and Docosahexaenoic) fatty acids after 48 h of incubation citrate-capped Ag NPs and Au NPs were observed. The total unsaturated fatty acid level changed from 55.11 ± 1.18 % mol for the control, to 46.47 ± 6.01 % mol after exposure to the citrate-coated Ag NPs, and to 51.7 ± 6.2 % mol after exposure to the polyphenol-capped Ag NPs. The trend was similar on saturated fatty acids when cells were exposed to citrate-coated Ag NPs. The levels of the unsaturated fatty acids seemed generally more susceptible to the NPs activity (**Table 3**).

Fatty Acids		CTRL (% mol)	Polyphenol-capped Au NPs (% mol)	Polyphenol-capped Ag NPs (% mol)	Citrate-capped Au NPs (% mol)	Citrate-capped Ag NPs (% mol)
Myristic	C 14:0	0.25 ± 0.1	0.23 ± 0.12	0.24 ± 0.13	0.17 ± 0.59	0.15 ± 0.8
Palmitic	C 16:0	16.5 ± 3.25	16.0 ± 1.25	16.08 ± 2.5	15.89 ± 0.5	15.80 ± 1.5
Palmitoleic	C 16:1	0.59 ± 0.05	0.49 ± 0.02	0.47 ± 0.05	0.38 ± 0.08	0.31 ± 0.06
Stearic	C 18:0	12.01 ± 3.05	8.88 ± 2.05	8.58 ± 1.01	9.55 ± 1.3	7.53 ± 2.3
Oleic	C 18:1	8.95 ± 2.2	8.5 ± 1.4	8.61 ± 3.2	7.3 ± 1.5	6.85 ± 1.2
Linoleic	C 18:2	20.83 ± 2.4	18.35 ± 3.2	17.9 ± 1.02	18.2 ± 1.6	17.8 ± 3.4
Arachidonic	C 20:4	20.3 ± 3.6	20.01 ± 2	19.75 ± 1.85	18.23 ± 2.3	18.01 ± 1.3
Eicosapentaenoic	C 20:5	1.01 ± 0.025	0.89 ± 0.20	0.81 ± 0.075	0.78 ± 0.083	0.72 ± 0.03
Docosapentaenoic	C 22:5	0.30 ± 0.014	0.28 ± 0.022	0.25 ± 0.024	0.22 ± 0.023	0.18 ± 0.04
Docosahexaenoic	C 22:6	3.12 ± 0.11	3.1 ± 1.012	3.9 ± 0.025	2.8 ± 1.3	2.6 ± 0.3
∑ saturated		28.76 ± 2.13	25.14 ± 2.05	24.9 ± 2.9	25.61 ± 1.5	23.84 ± 3.1
∑ insaturated		55.11 ± 1.18	51.62 ± 0.98	51.69 ± 6.2	47.91 ± 0.86	46.47 ± 6.01

Table 3. Fatty acids analysis phospholipids in mitochondrial membranes of HL7702 cells induced by 48 h of exposure to c2 polyphenol- and citrate-capped Au NPs and Ag NPs. Results are calculated as mean of five experiments ± DS and they considered statistically significant performing a student's t-test with a p values < 0.05 (<0.05 *).

The changes in phospholipids and fatty acids chain has been found to modify the lipid-lipid interactions, membrane permeability, ion gradients and membrane fluidity inducing a decreasing of the membrane thickness (Agmon et al 2018; Wong-Ekkabut et al. 2007). In addition, changes in the phospholipids content were demonstrated to be involved in the import and assembly of proteins through membranes. Moreover, they are crucial for tubular mitochondrial morphology and membrane fusion (Choi et al. 2006; Steenbergen et al. 2005). It has been demonstrated that mitochondrial morphology depends on a balance between fusion and fission events. The GTPase cytosolic dynamin-related protein-1 (Dpr-1) regulates the fission phenomena, translocating to the outer mitochondrial membrane and inducing the development of active fission sites. The speed of fission could derive from overexpression of Dpr-1 that can reduce ATP efficiency. These dynamics are crucial for regulating cell death or survival, because they are essential for cellular development and homeostasis, as well as apoptosis (Otera and Ishihara 2013). Previous works analysed the NPs effect on Dpr-1 expression in tumoral cell lines demonstrated the induction of endothelial injury via Drp-1 (Guo et al. 2018) as well as Au NPs in lung cancer cells (Ke et al 2017). We then explored here a potential correlation between the presence of phospholipids with the fission events by studying the regulation of Dpr-1. A higher decrease of phospholipids/fatty acids, together with a hyperexpression of Dpr-1, has been found after cell exposure to citrate-coated Au NPs and Ag NPs compared to polyphenol-capped Au NPs. The impressive increase observed in the fission process may impair the physiological mitochondrial network, remodelling them or even changing their turnover (Fix et al. 2019; Suárez-Rivero et al. 2017). Immunoblot analyses of Dpr-1 on liver cells showed that the Drp-1 levels were markedly higher in cells after 48 h of treatment with c2 citrate-capped Au NPs and Ag NPs (**Figure 6a**). In particular, the expression increased up to 155 % ± 25 in cells treated with Ag NPs. The polyphenol-capped NPs did not induce several overexpression, suggesting a negligible effect on the regulation of Dpr-1 (**Figure 6b**).

Figure 6. a. Western blot and (**b**) densitometric analysis of Dpr-1 expression of HL7702, after 48 h of exposure to c2 polyphenol- and citrate—coated Au NPs and Ag NPs. The reported values are estimated as average of five independent

471 experiments ± SD and they considered statistically significant performing a student's t-test with a p values < 0.05 (<0.05
472 *).

473

474

475 It is likely that the alteration of the lipid composition of the mitochondrial membranes, as well as the changes in the fission
476 process can influence the susceptibility of the membranes to ROS. This can in turn stimulated lipid peroxidation and
477 result in the formation of MDA after exposure to Au NPs and Ag NPs at the highest concentration. the ROS production
478 in HL7702 cell after 24 h and 48 h of exposure to c1 and c2 polyphenol-capped and citrate coated Au NPs and Ag NPs
479 were investigated (**Figure 7a**). As expected, the levels of ROS were dose and time dependent and were strictly linked to
480 the synthetic route used. In agreement with the previous data, the incubation with polyphenol-capped Au NPs and Ag
481 NPs did not induce a strong ROS production. In fact, the maximum percentage was 118 % compared to control in cells
482 incubated with c2 polyphenol-capped AgNPs after 48 h. Conversely, the NPs obtained by the colloidal chemical route
483 led to high levels of ROS. In this case, the citrate-coated Au NPs induced an increase of 128 % ± 9 of ROS at the highest
484 concentration tested after 48 h, whereas the citrate-capped Ag NPs lead to values of 155 ± 12%. The MDA-based assay
485 was used to check potential ROS-mediated lipid peroxidation. The cellular levels of MDA grew up after exposure to the
486 two types of NPs, and this was more remarkable for the citrate-coated metal NPs. High levels of MDA have been produced
487 by the cell after 48 h of exposure to c2 NPs, corresponding to ca. 7.3 ± 0.2 nmol mg^{-1} for the citrate-coated Ag NPs and
488 4.80 ± 1.02 nmol mg^{-1} for the citrate-coated Au NPs, with respect to the 2.3 ± 0.8 nmol mg^{-1} of the control (**Figure 7b**).
489 The polyphenol-coated NPs did not dramatically affect the MDA levels. The increased MDA levels were proportional to
490 the concentration and exposure time, in close agreement with the performed assays. The increase of oxidized lipids in
491 mitochondrial membranes was related to a decrease in membrane fluidity and slower lateral diffusion (Otera and Ishihara
492 2013). In addition, fission and fusion events have been found to combine with mitochondrial mass control to determine
493 the mitochondrial morphology (Favaro et al. 2019; Huang and Galloway 2011). Our results suggested a possible damage
494 of mitochondrial membranes that can be eventually ascribed to the organelles swell and loss of their morphological
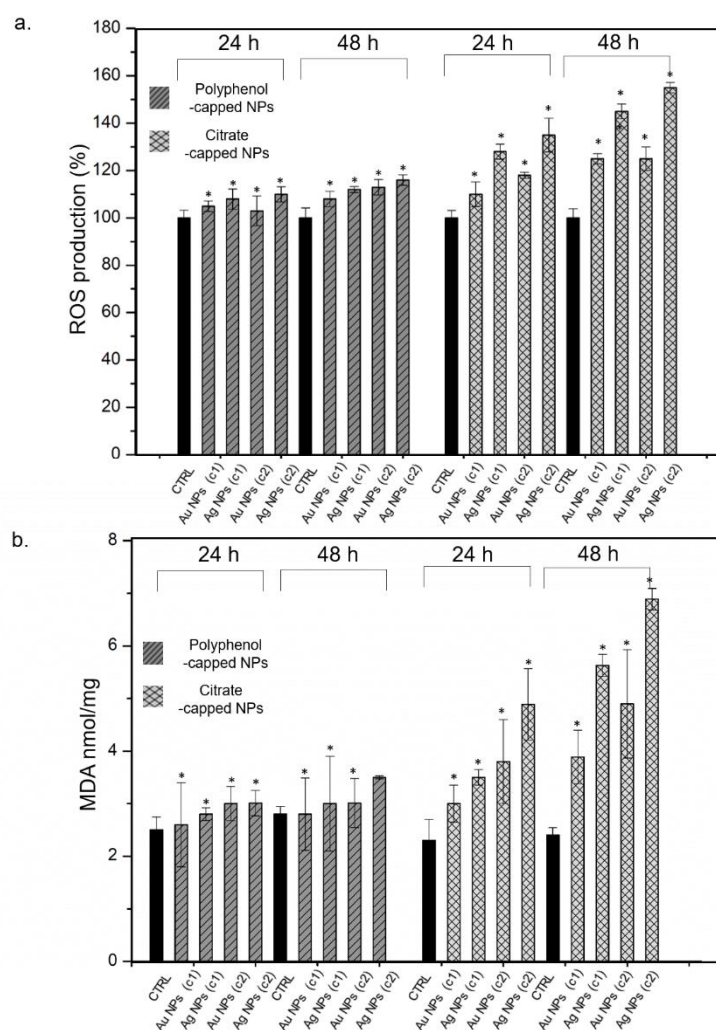495 characteristics (Kowaltowskia 1999).

Figure 7. a. ROS and **b** MDA levels after 24 h and 48 h HL7702 cells exposure to c1 and c2 polyphenol- and citrate-coated Au NPs and Ag NPs.

To confirm a possible damage-induced change of mitochondrial morphology HL7702 mitochondria were labelled with MitoTracker™, before (**Figure 8a**) and after 48 h of exposure to c2 polyphenol- (**Figure 8 b,c**) and citrate-coated NPs (**Figure 8 d,e**).
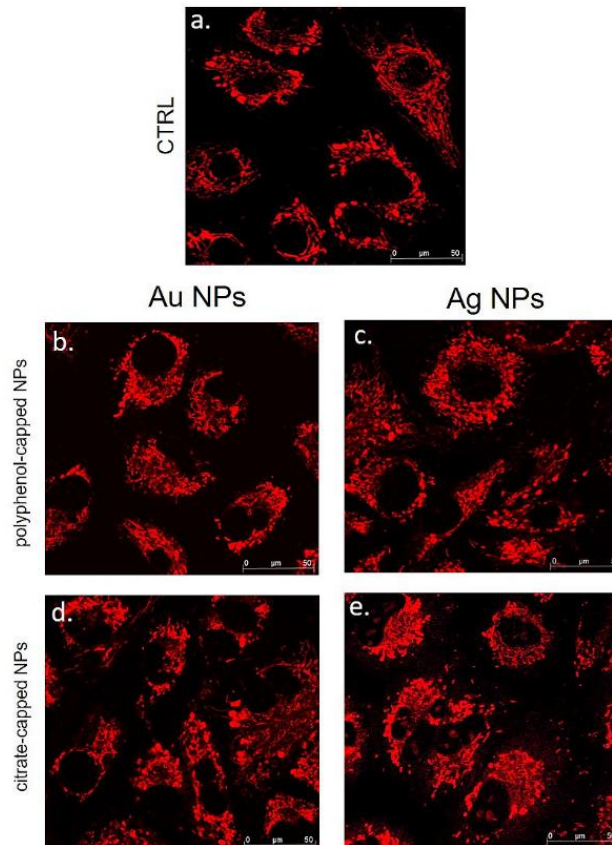
Figure 8. Confocal microscope images of HL7702 cells labeled with MitoTracker™ Orange. Control cells (**a**), cells after 48 h of treatment with c2 polyphenol- (**b.c**) and citrate– (**d,e**) capped Au NPs and Ag NPs.

The confocal analyses showed organelles that are shorter and more circular than control (untreated) cells, indicating a loss of structural integrity in response to the NPs exposure. This was again particularly evident for the NPs derived by the colloidal chemical route, where the strongest change of morphology were observed. The "Mito Morphology" macro text file plug-in of ImageJ software (Dagda et al 2009) provided an estimation of the circularity (index of elongation) of untreated HL7702 mitochondria of ca. 0.140 ± 0.003 and the mitochondria displayed also an elongated shape (**Figure 9**). Such a value decreased down to 0.180 ± 0.002 and 0.195 ± 0.030 for HL7702 mitochondria treated with the polyphenol-capped Au NPs and Ag NPs, respectively, while the mitochondria tended to a more spherical shape. After cells incubation with the citrate-coated Au and Ag NPs, the circularity significantly decreased down to 0.250 ± 0.005 and 0.39 ± 0.02, and mitochondria showed a more evident spherical shape (**Figure 9a**). The changes of the mitochondria morphology induced by Au and Ag NPs have been also reported as mitochondrial average area/perimeter ratio, which was normalized to the circularity and to the minor axis in order to account for swollen mitochondria that attain a large area and may be mixed with interconnected mitochondria. The average area/perimeter ratio normalized to the minor axis (assuming that mitochondria are considered as ellipses) accounts for conditions that can induce mitochondrial swelling. Normalizing to circularity, such value was ca. 7.0 ± 0.2 for the untreated cells and it slightly decreased down to 6.3 ± 0.3 and 6.10 ± 0.08 after exposure to polyphenol-capped Au NPs and Ag NPs and switched to 4.8 ± 0.5 and 3.000 ± 0.005 after treatment with the citrate–coated Au NPs and Au NPs, respectively (**Figure 9b**). Normalizing to the minor axis, the value recorded

21

for the HL7702 negative control resulted 0.140 ± 0.008, and it slightly increased up to 0.17 ± 0.05 and 0.18 ± 0.10, after exposure with the polyphenol-capped Au NPs and Ag NPs, respectively. Conversely, the citrate-capped Au NPs and Ag NPs resulted in a higher increase, namely 0.21 ± 0.03 and 0.32 ± 0.05, respectively (**Figure 9c**).
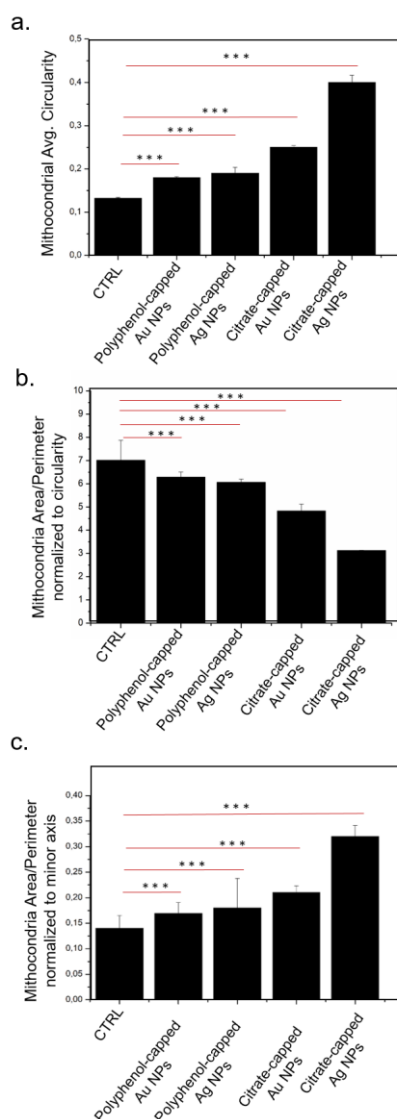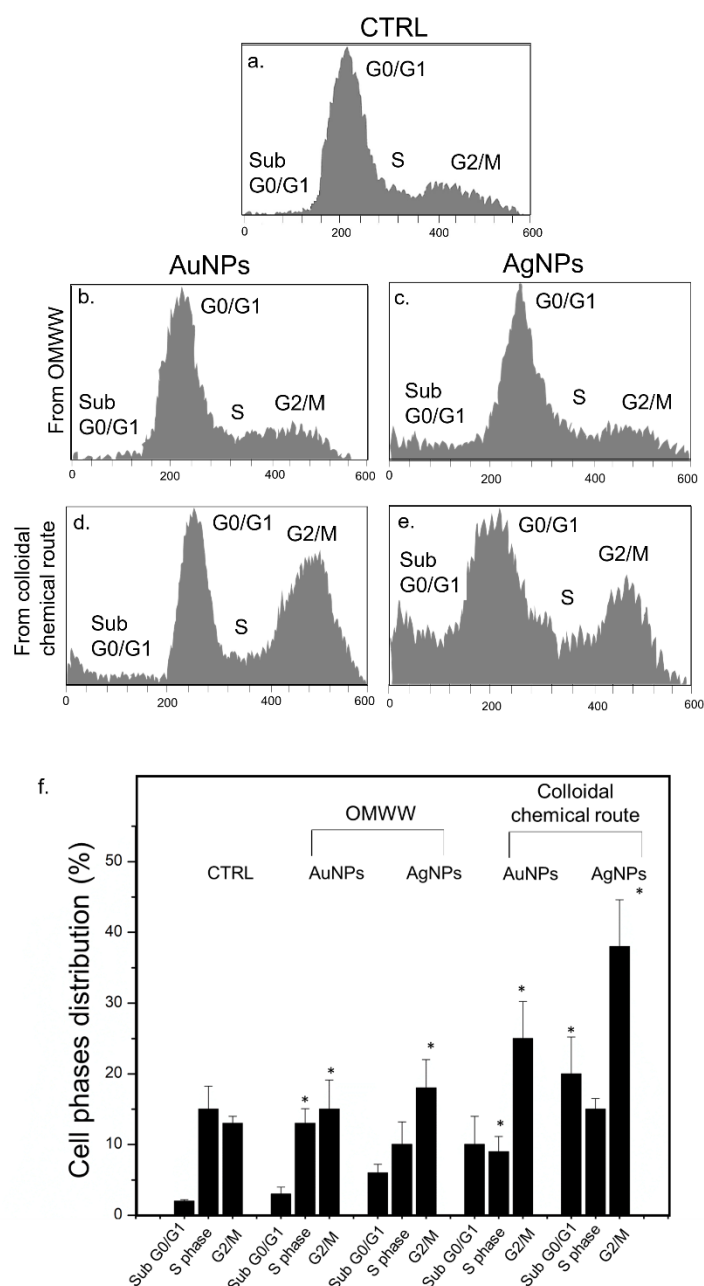

Figure 9. Mean values and standard deviations of mitochondrial average circularity (**a**) mitochondria area/perimeter normalized to circularity (**b**) and mitochondria area/perimeter normalized to minor axis (**c**) of HL7702 untreated and treated for 48 h with c2 of green polyphenols-capped and colloidal Au NPs and Ag NPs .

The observed results can be associated to mitochondria fission (Randy et al. 2012) and could cause mitochondrial swelling, which in turn leads to oxidative stress. On the other hand, NPs achieved from OMWW seemed to induce only mild changes in mitochondria characteristics, suggesting their low toxicity and tolerance in healthy cells, probably due to the presence of the polyphenol shell. In light of these results, the analyses of cell cycle have been performed to evaluate the link between mitochondrial damage, upon exposure to NPs, and the cell cycle progression. During cellular proliferation, the G1 phase is characterized by the biosynthesis of cellular components, a process supported by the energy produced by mitochondria (Antico et al. 2012). After the G1, the S/G2/M phase is characterized by biosynthesis of

22

mitochondria and DNA replication (Martínez-Diez et al. 2006). In order to understand if NPs inducing damage to mitochondria, can also altered the cell cycle, we performed flow cytometry on HL7702 in order to define the cells percentages in the cell cycle sub G0/G, G0/G1, S, and G2/M, before (**Figure 10 a**) and after 48 h of treatment with c2 polyphenol-capped Au NPs and Ag NPs (**Figure 10 b, c**) and citrate-coated AuNPs and AgNPs (**Figure 10 d, e**). The NPs derived from the colloidal chemical route, and the Ag NPs in particular, strongly affected the cell cycle progression. 14 ± 4 % of untreated cells (control) were in the in G2/M phase, while 15 ± 4 % and 18 ± 3 % of cells were in the same G2/M phase after treatment with polyphenol-capped Au NPs and Ag. We also observed 15 ± 3 % of untreated cells in the S phase, and this percentage passed to 13 ± 2 % and 10 ± 3 % after treatment with polyphenol-capped Au NPs and Ag NPs (**Figure 10 f**). In addition, we found 3 % ± 1 for polyphenol-coated Au NPs and 6 % ± 1 of polyphenol-capped Ag NPs in G0/G1 transition, and 2.5 ± 0.6 % of untreated cells. On the other hand, the exposure to citrate-coated Au and citrate-capped Ag NPs induced accumulation of cells in G2/M and sub G0/G1 with respect to S phase (**Figure 10 f**). In details, we found 25 ± 5.2 % of cells in G2/M and of 10 ± 4 % in sub G0/G1 phase after citrate-Au NPs incubation, whereas the values became remarkably higher after citrate-capped Ag NPs treatment. In this case, 38 ± 6 % of cells were in G2/M phase and 20 % ± 5 in the sub G0/G1 transition. Cells in S phase are 9 % ± 2 and 15 % ± 1 after treatment with citrate-Au NPs and citrate-Ag NPs, respectively. These results assessed that the citrate-capped NPs induced apoptosis and inhibited cell grown (**Figure 10 f**). The overexpression of Drp-1, together with the toxic effects recorded in cells after NPs exposure (with particular reference to NPs obtained from colloidal chemical route) promoted the cells towards the G2/M and sub G0/G1 phase of the cell cycle, hypothesizing a G2-M apoptosis in HL77002 cells. These results showed a relatively higher toxicity of the citrate-coated metal NPs, while the polyphenol-coated metal NPs were more tolerated by liver cells.

Figure 10. a. Flow cytometry cell cycle distribution in HL7702 cells before (a) and after 48 h of treatment with c2 polyphenol- (**b,c**) and citrate-coated Au NPs and Ag NPs (**d,e**) and cell cycle distribution (%) in Sub G0/G1, S and G2/M phases (**f**).

4. Conclusion

Au and Ag NPs from a widespread waste in the Mediterranean regions were obtained here, that represents a serious environmental problem due to the high pollutants load. This waste was valorised using it as a source of reducing and capping agents suitable for the synthesis of plasmonic NPs. This procedure also led to the reduction of polluting substances and a consequent purification of OMWW, with the possibility to dispose it in the environment and reuse as source of irrigation. In addition, this green synthesis enable obtaining high stable NPs due to the polyphenol shell. In

24

addition, these green NPs did not induced significant perturbations in cells especially at the mitochondrial level in healthy cells. Conversely, the NPs obtained from conventional colloidal chemical synthesis triggered a strong alteration of the phospholipids bilayer, in terms of fatty acids mis-regulation and in the process of mitochondrial fission through the hyper expression of the Drp-1 protein. The next experimental goals will be the use of these green Au NPs and Ag NPs on tumor cell lines, in order to understand their potential inhibitor effect on cancer progression pathways being confident of their non-toxicity on healthy cells. Ag NPs can trigger apoptotic response in cancer cells due to Ag ions release whereas Au NPs can be used for *in vivo* photothermal therapy in cancer treatment.

Declarations

Ethics approval and consent to participate: not applicable.

Consent for publication: not applicable.

Availability of data and materials: not applicable.

Competing interests: The authors declare no conflict of interest.

Funding: The authors received no specific funding for this work.

References

Acton BM, Jurisicova A, Jurisica I, Casper RF (2004). Alterations in mitochondrial membrane potential during preimplantation stages of mouse and human embryo development. Mol Human Reprod 10(1):23–32.

Adhoum NML (2004). Decolourization and removal of phenolic compounds from olive mill wastewater by electrocoagulation. Chem Eng Process 43:1281–12.

Aggoun M, Arhab R, Cornu A, Portelli J, Barkat M, G. B (2016) Olive Mill Wastewater Microconstituents Composition According to Olive Variety and Extraction Process. Food Chem 15(209):72-80.

Agmon E, Solon J, Bassereau P et al (2018) Modeling the effects of lipid peroxidation during ferroptosis on membrane properties. Sci Rep 8:5155.

Alegria ECBA, Ribeiro APC, Mendes M, Ferraria AM, Do Rego AMB PA (2018) Effect of Phenolic Compounds on the

Synthesis of Gold Nanoparticles and its Catalytic Activity in the Reduction of Nitro Compounds. Nanomaterials (Basel) 8(5):320.

Antico VG, Elguero ME, Poderoso JJ, Carreras MC (2012) Mitochondrial Regulation of Cell Cycle and Proliferation. Antioxid Redox Signal. 16(10): 1150–1180.

Balis K, Chatzipavlidis I, Antonakou M et al (1955) Study of the methods and processes for OMW treatment with the goal to prevent environmental pollution and final disposal to the sea, study under project funded under the LEADER European Union initiative, Agricultural University of Athens. Athens: General.

Bao Z, Cao J, Kang G et al (2019) Effects of reaction conditions on light-dependent silver nanoparticle biosynthesis mediated by cell extract of green alga Neochloris oleoabundans. Environ Sci Pollut Res 26:2873–2881.

Barth PG, Scholte HR, Berden JA et al (1983) An X-linked mitochrondrial disease affecting cardiacmuscle, skeletalmuscle and neutrophil leucocytes. J Neurol Sci 62(1–3):327–355.

Berliner JA, Leitinger N, Tsimikas T (2009) The role of oxidized phospholipids in atherosclerosis. J of Lipid Res 50:S207–S212.

Bligh EG, Dyer W (1959) A rapid method of total lipid extraction and purification. Can J Biochem Physio 37:911–917.

Bradford M (1976) A rapid and sensitive method for the quantitation of microgram quantities of protein utilizing the principle of protein-dye binding. Anal Biochem 72:248–254.

Chatzisymeon E, Diamadopoulos E, Mantzavinos D (2009) Effect of key operating parameters during wet oxidation of olive mill wastewaters. Water Sci Technol 59(12):2509e2518.

Chatzisymeon E, Foteinis S, Mantzavinos D, Tsoutsos T (2013) Life cycle assessment of advanced oxidation processes for olive mill wastewater treatment. J Cleaner Prod, 54, 229e234.

Chatzisymeon E, Xekoukoulotakis NP, Mantzavinos D (2009) Determination of key operating conditions for the photocatalytic treatment of olive mill wastewaters. Catalysis T 144(1–2):143–148.

Choi S, Huang P, Jenkins G. et al (2006) A common lipid links Mfn-mediated mitochondrial fusion and SNARE-regulated exocytosis. Nature Cell Biol 8(11):1255–1262.

CNR-IRSA. (2003) Metodi analitici per le acque.

Daâssi D, Sellami S, Frikha F, Rodriguez-Couto S, Nasri M, Mechichi T (2016) Assessment of Coriolopsis gallica-treated olive mill wastewater phytotoxicity on tomato plants. Environ Sci Pollut Res 23(15):15370–15380.

Dagda RK, Cherra SJ, Kulich SM, Tandon A, Park D, Chu CT (2009) Loss of PINK1 Function Promotes Mitophagy through Effects on Oxidative Stress and Mitochondrial Fission. J Biol Chem 284(20):13843–13855.

Dauthal P, Mukhopadhyay M (2016) Noble Metal Nanoparticles: Plant-Mediated Synthesis, Mechanistic Aspects of Synthesis , and Applications. Ind Eng Chem Res 55:36, 9557–9577.

De Almeida MS, Martins RC, Quinta-Ferreira RM et al (2018) Optimization of operating conditions for the valorization of olive mill wastewater using membrane processes. Environ Sci Pollut Res 25:21968–21981.

639 De Leonardis A, Macciola V, Lembo G, Aretini A, Nag A (2007) Studies on oxidative stabilisation of lard by natural
640   antioxidants recovered from olive-oil mill wastewater. Food Chem 100:998–1004.

641 De Matteis V, Malvindi MA, Galeone A, Brunetti V, De Luca E, Kote S, Kshirsagar P, Sabella S, Bardi G, Pompa PP
642   (2015) Negligible particle-specific toxicity mechanism of silver nanoparticles: The role of Ag + ion release in the
643   cytosol. Nanomedicine 11(3):731–739.

644 De Matteis V, Rizzello L, Di Bello MP, Rinaldi R (2017) One-step synthesis, toxicity assessment and degradation in
645   tumoral pH environment of SiO2@Ag core/shell nanoparticles. J Nanop Res 19(6), 14.

646 De Matteis V, Rizzello L, Ingrosso C, Liatsi-Douvitsa E, De Giorgi ML, De Matteis G, Rinaldi R (2019) Cultivar-
647   Dependent Anticancer and Antibacterial Properties of Silver Nanoparticles Synthesized Using Leaves of Different
648   Olea Europaea Trees. Nanomaterials 9(11):1544.

649 De Matteis V, Cascione MF, Toma CC, Pellegrino P, Rizzello L, Rinaldi R (2019) Tailoring Cell Morphomechanical
650   Perturbations Through Metal Oxide Nanoparticles. Nanoscale Res Lett 14(109).

651 Dutournié P, Jeguirim M, Khiari B, Goddard ML, Jellali S (2019) Olive Mill Wastewater: From a Pollutant to Green
652   Fuels, Agricultural Water Source, and Bio-Fertilizer. Part 2: Water Recovery. Water 11(4):738.

653 El Hajjouji H, Barje F, Pinelli E, Bailly JR, Richard C, Winterton P, Revel JR, Hafidi F (2008) Photochemical UV/TiO2
654   treatment of olive mill wastewater (OMW). Bioresour Technol 99(15):7264-9.

655 Enaime G, Baçaoui A, Yaacoubi A et al (2020) Phytotoxicity assessment of olive mill wastewater treated by different
656   technologies: effect on seed germination of maize and tomato. Environ Sci Pollut Res 27:8034–8045.

657 Favaro G, Romanello V, Varanita T et al (2019) DRP1-mediated mitochondrial shape controls calcium homeostasis and
658   muscle mass. Nat Commun 10:2576.

659 Fiske CH, Subbarow Y (1925) The colorimetric determination of phosphorus. Biochem J 66:375-400.

660 Fix DK, VanderVeen BN, Counts BR, Carson JA (2019) Regulation of Skeletal Muscle DRP-1 and FIS-1 Protein
661   Expression by IL-6 Signaling. Ox Med Cel Long 12:ID 8908457.

662 Flouri C, Chatzipavlidis I, Balis K, et al (1988) Olive mill wastewater application to soil. In: Ministry of the Aegean,
663   editor. In: Ministry of the Aegean, Editor. Proceedings of Scientific Conference on Aegean Olive Trees. 27/2/88.
664   Mytilene: Eleourgiki, P.E.

665 Giedt RJ, Pfeiffer DR, Matzavinos A, Kao CY, Alevriadou BR (2012) Mitochondrial Dynamics and Motility Inside
666   Living Vascular Endothelial Cells: Role of Bioenergetics. Ann Biomed Eng 40:(1903–1916).

667 Goldfar JL, Buessing L, Gunn E, Lever M, Billia A, Casoliba E, Schievano A, Adani F (2017) Novel Integrated
668   Biorefinery for Olive Mill Waste Management: Utilization of Secondary Waste for Water Treatment. ACS
669   Sustainable Chem. Eng. 5(1):876–884.

670 Guo C, Wang J, Jing L, Ma R, Liu X, Gao L, Cao L, Duan J, Zhou X, Li Y, Sun Z (2018) Mitochondrial dysfunction,
671   perturbations of mitochondrial dynamics and biogenesis involved in endothelial injury induced by silica
672   nanoparticles. Environ Pollut 236:(926–936).

Hamimed S, Jebli N, Sellami H, Landoulsi S, Chatti A (2020) Dual Valorization of Olive Mill Wastewater by Bio-Nanosynthesis of Magnesium Oxide and Yarrowia lipolytica Biomass Production. Chem Bio 17(3).

Hammad LA, Wu G, Saleh MM, Klouckova I, Dobrolecki LE, Hickey RJ, Schnaper L, Novotny M, Mechref Y (2009) Elevated levels of hydroxylated phosphocholine lipids in the blood serum of breast cancer patients. Rapid Commun Mass Spectrom 23(6):863–876.

Holte LL, van Kuijk FJ, Dratz EA (1990) Preparative high-performance liquid chromatography purification of polyunsaturated phospholipids and characterization using ultraviolet derivative spectroscopy. Anal Biochem 188(1):136–141.

Huang P, Galloway CA, Yoon Y (2011) Control of mitochondrial morphology through differential interactions of mitochondrial fusion and fission proteins. PLoS One 6(5):e20655.

Ichihara K, Fukubayashi Y (2010) Preparation of fatty acid methyl esters for gas-liquid chromatography. J Lipid Res 51(3):635–640.

Isidori M, Lavorgna M, Nardelli A, Parrella A (2005) Model study on the effect of 15 phenolic olive mill wastewater constituents on seed germination and Vibrio fischeri metabolism. J Agric Food Chem 19(53(21):8414–8417.

Kagan VE, Tyurin VA, Jiang J, et al (2005) Cytochrome c acts as a cardiolipin oxygenase required for release of proapoptotic factors. Nature Chem Bio 1(4):223–232.

Ke S, Zhou T, Yang P, et al (2017) Gold nanoparticles enhance TRAIL sensitivity through Drp1-mediated apoptotic and autophagic mitochondrial fission in NSCLC cells. Int J Nanomed 12:2531–2551.

Kowaltowskia AJ, Vercesi A (1999) Mitochondrial damage induced by conditions of oxidative stress. Free Rad Bio Med 26(3–4):463–471.

Li S, Tan HY, Wang N, Cheung F, Hong M, Feng Y (2018) The Potential and Action Mechanism of Polyphenols in the Treatment of Liver Diseases. Oxid Med Cell Longev 8394818.

Lichtenthaler HK, Buschmann C (2001) Chlorophylls and carotenoids measurement and characterization by UV–VIS. Current Protocols in Food Analytical Chemistry (CPFA), 1, 1 F4.3.1–F4.3.8.

López-Piñeiro A, Murillo S, Barreto C, Muñoz A, Rato JM, A Albarrán A, Garcìa A (2007) Changes in organic matter and residual effect of amendment with two-phase olive-mill waste on degraded agricul- tural soils. Sci Total Environ 378(1-2):84–89.

MacKinney G (1941) Absorption of light by chlorophyll solutions. J Biol Chem 140:315–322.

Maiorano G, Rizzello L, Malvindi MA, Shankar SS, Martiradonna L, Falqui A, Cingolani R, Pompa PP (2013) Monodispersed and size-controlled multibranched gold nanoparticles with nanoscale tuning of surface morphology. Nanoscale 3:2227–2232.

Mantzavinos D, Kalogerakis N (2005) Treatment of olive mill effluents: part I. Organic matter degradation by chemical and biological processes e an overview. Environm Internat 31(2):289e295.

707 Martínez-Diez M, Santamaría G, Ortega AD, Cuezva J (2006) Biogenesis and Dynamics of Mitochondria during the Cell
708   Cycle: Significance of 3′UTRs. PLoS One 1(1):e107.

709 McNamara CJ, Anastasiou CC, O'Flahertyd V, Mitchell R (2008) Bioremediation of olive mill wastewater. Nt
710   Biodeterior Biodegrad 61:127–134.

711 Mert BK, Yonar T, Kiliç MY, Kestio glu K (2010) Pre-treatment studies on olive oil mill effluent using physicochemical,
712   Fenton and Fenton-like oxidations processes. J Haz Mat 174(1e3):122e128.

713 Montine TJ, Montine KS, McMahan W, Markesbery WR, Quinn JF, Morrow JD (2005) F2-isoprostanes in Alzheimer
714   and other neurodegenerative diseases. Antiox Redox Sig 7(1-2,), 269–275.

715 Nakamura GR (1952) Microdetermination of phosphorus. Anal Chem 24:1372.

716 Nassar NN, Arar LA, Marei NN, Abu MM, Dwekat MS, Sawalha SH (2014) Treatment of olive mill based wastewater
717   by means of magnetic nanoparticles: Decolourization, dephenolization and COD removal. Envir Nanotech Monit
718   Manag 1–2:14–23.

719 Niaounakis M, H Halvadakis C (2006) Olive Processing Waste Management, Volume 5 2nd Edition Literature Review
720   and Patent Survey. Elsevier, 9780080448510.

721 Nogueira V, Lopes I, Rocha-Santos T, Gonçalves F, Duarte AC, Pereira R (2016) Photocatalytic Treatment of Olive Oil
722   Mill Wastewater Using TiO_2 and Fe_2O_3 Nanomaterials. Water, Air, Soil Pol 227(88).

723 Otera H, Ishihara N, Mihara K (2013) New insights into the function and regulation of mitochondrial fission. Biochim
724   Biophys Acta 1833(5):1256–1268.

725 Ouzounidou G, Zervakis GI, Gaitis F (2010) Raw and microbiologically detoxified olive mill waste and their impact on
726   plant growth. Terr Aquatic Environ Toxicol 4(1):21–38.

727 Rahmanian N, Jafari SM, Galanakis CM (2014) Recovery and Removal of Phenolic Compounds from Olive Mill
728   Wastewater. J Am Oil Chem Soc 91:1–18.

729 Ramos-Cormenzana A, Juarez-Jimenez B, Garcia-Pareja MP (1996) Antimicrobial activity of olive mill waste-waters
730   (alpechín) and biotransformed olive oil mill wastewater. Int Biodeterior Biodegrad 38:283–290.

731 Rozzi A, Malpei F (1996) Treatment and disposal of olive mill effluents. Int Biodeterior Biodegrad 38:135–144.

732 Rusan MJM, Albalasmeh AA, Malkawi HI (2016) Treated Olive Mill Wastewater Effects on Soil Properties and Plant
733   Growth. Water Air Soil Pollut 227(135).

734 Sarika R, Kalogerakis N, Mantzavinos D (2005) Treatment of olive mill effluents: part II. Complete removal of solids by
735   direct flocculation with poly-electrolytes. Environ Int 31:297–304.

736 Singh J, Dutta T, Kim K et al (2018) 'Green' synthesis of metals and their oxide nanoparticles: applications for
737   environmental remediation. J Nanobiotechnol 16(84).

738 Singleton VL, Rossi JA (1965) Colorimetry of total phenolics with phosphomolybdic-phosphotungstic acid reagents. Am
739   J Enol Vitic16(3):144–158.

740   Smirnova E, Shurland DL, Ryazantsev SN, van der Bliek AM (1998) A human dynamin-related protein controls the
741   distribution of mitochondria. J Cell Biol 143:351–358.

742   Souilem S, El-Abbassi A, Hafidi HA, Sayadi S, Galanakis C (2017) Olive oil production sector: environmental effects
743   and sustainability challenges. In Olive Mill Waste-Recent Advances for Sustainable Management ISBN
744   9780128053140 1–28.

745   Steenbergen R, Nanowski TS, Beigneux A, Kulinski A, Young SG, Vance JE (2005) Disruption of the phosphatidylserine
746   decarboxylase gene in mice causes embryonic lethality and mitochondrial defects. J Biol Chem 280(48):40032–
747   40040.

748   Suárez-Rivero JM, Villanueva-Paz M, de la Cruz-Ojeda P, et al (2017) Mitochondrial Dynamics in Mitochondrial
749   Diseases. Diseases 5(1):1.

750   Technical Committee: ISO/TC 147/SC 2 Physical, chemical and biochemical methods (2002) Water quality —
751   Determination of the chemical oxygen demand index (ST-COD) — Small-scale sealed-tube method.

752   Torrecilla JS (2010) Phenolic Compounds in Olive Oil Mill Wastewater. In Olives and Olive Oil in Health and Disease
753   Prevention. Elsevier Inc. ISBN 978-0-12-374420-3.

754   Tsagaraki E, Lazarides HN, PK. (2007). Olive mill wastewater treatment in utilization of by-products and treatment of
755   waste in the food industry. Springer Berlin (133–157).

756   Wong-Ekkabut J, Xu Z, Triampo W, Tang IM, Tieleman DP, Monticelli L (2007) Effect of Lipid Peroxidation on the
757   Properties of Lipid Bilayers: A Molecular Dynamics Study. Biophys J. 2, *93*(12):4225–4236.

758   Yin H, Zhu M (2012) Free radical oxidation of cardiolipin: chemical mechanisms, detection and implication in apoptosis,
759   mitochondrial dysfunction and human diseases. Free Radic Res 46(8):959–974.
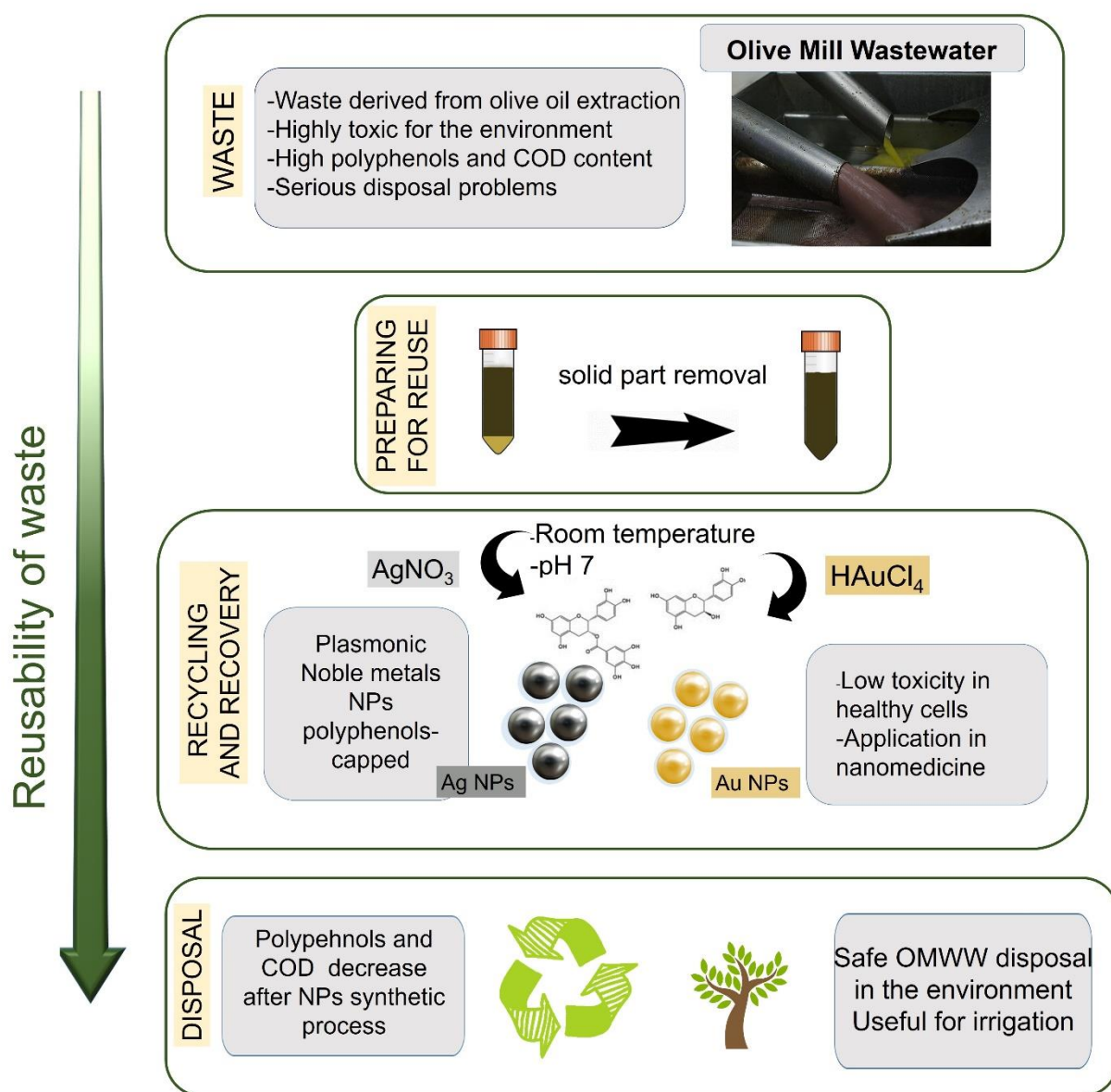
760

761

762

763

764

765

766

767

768

769

770

771

774

Graphical Abstract

776

777

778
779
780

781

782

783